Geophys. J. Int. (2009) **176,** 589–600 doi: 10.1111/j.1365-246X.2008.04001.x

Spectral modification of seismic waves propagating through solids exhibiting a resonance frequency: a 1-D coupled wave propagation–oscillation model

Marcel Frehner,[1] Stefan M. Schmalholz[1] and Yuri Podladchikov[2]

[1] *Geological Institute, Department of Earth Sciences, ETH Zurich, Switzerland. E-mail: marcel.frehner@erdw.ethz.ch*
[2] *Physics of Geological Processes (PGP), University of Oslo, Norway*

Accepted 2008 October 05. Received 2008 August 15; in original form 2007 October 12

SUMMARY

A 1-D model is presented that couples the microscale oscillations of non-wetting fluid blobs in a partially saturated poroelastic medium with the macroscale wave propagation through the elastic skeleton. The fluid oscillations are caused by surface tension forces that act as the restoring forces driving the oscillations. The oscillations are described mathematically with the equation for a linear oscillator and the wave propagation is described with the 1-D elastic wave equation. Coupling is done using Hamilton's variational principle for continuous systems. The resulting linear system of two partial differential equations is solved numerically with explicit finite differences. Numerical simulations are used to analyse the effect of solids exhibiting internal oscillations, and consequently a resonance frequency, on seismic waves propagating through such media. The phase velocity dispersion relation shows a higher phase velocity in the high-frequency limit and a lower phase velocity in the low-frequency limit. At the resonance frequency a singularity in the dispersion relation occurs. Seismic waves can initiate oscillations of the fluid by transferring energy from solid to fluid at the resonance frequency. Due to this transfer, the spectral amplitude of the solid particle velocity decreases at the resonance frequency. After initiation, the oscillatory movement of the fluid continuously transfers energy at the resonance frequency back to the solid. Therefore, the spectral amplitude of the solid particle velocity is increased at the resonance frequency. Once initiated, fluid oscillations decrease in amplitude with increasing time. Consequently, the spectral peak of the solid particle velocity at the resonance frequency decreases with time.

Key words: Numerical solutions; Fourier analysis; Wave propagation; Acoustic properties.

1 INTRODUCTION

A number of processes can cause oscillations with a resonance frequency within a heterogeneous rock. For example, the behaviour of non-wetting fluids entrapped in capillary tubes and in idealized pore spaces were studied (Dvorkin *et al.* 1990; Graham & Higdon 2000a; Graham & Higdon 2000b), and one of the main results is the oscillatory movement of the fluids when an external force is applied (Hilpert *et al.* 2000). The restoring force driving the oscillations is the surface tension force or capillary force. The result that isolated oil blobs in partially saturated rocks can exhibit a resonance frequency, motivated the suggestion of a new enhanced oil recovery method (EOR) termed 'wave stimulation of oil' or 'vibratory mobilization' (Beresnev & Johnson 1994; Iassonov & Beresnev 2003; Beresnev *et al.* 2005; Li *et al.* 2005; Hilpert 2007; Pride *et al.* 2008). Another example of solids exhibiting internal oscillations is cavities or other heterogeneities in solids. These heterogeneities can oscillate and exhibit a resonance frequency (Meyer *et al.* 1958; Anderson & Hampton 1980a; Anderson & Hampton 1980b; Landau & Lifschitz 1997). The process is also called resonant scattering (Werby & Gaunaurd 1989; Werby & Gaunaurd 1990; Hassan & Nagy 1997) and has applications in non-destructive testing of materials (Ida & Wang 1996; Castellini *et al.* 2000; Schultz *et al.* 2006). A third example of oscillatory behaviour is stratified media. Urquizu & Correig 2004 showed that under certain circumstances a seismic wave pulse propagating through a layered medium can be described mathematically with a differential equation for an oscillator.

The oscillating effects caused by heterogeneities or layered media are implicitly included in numerical models solving the full elastodynamic wave equations, as long as the heterogeneities or the layering are numerically well resolved (e.g. Frehner *et al.* 2008). However, the oscillatory behaviour of non-wetting fluid blobs in partially saturated rocks (e.g. Hilpert *et al.* 2000) is not included in mathematical models of wave propagation in partially saturated rocks. These models can be separated into two groups: (1) models based on Biot's equations (Biot 1962) for fully-saturated rocks,

applying a spatial variation of the pore fluid properties representing a partial saturation on the mesoscale (i.e. larger than the pore size and smaller than the wavelength; White 1975; Dutta & Ode 1979), and (2) models for three-phase (i.e. solid, wetting and non-wetting fluid) media considering a partial saturation on the pore scale, including particular capillary pressure versus saturation relations (Santos *et al.* 1990; Tuncay & Corapcioglu 1996; Smeulders & Van Dongen 1997; Wei & Muraleetharan 2002). In the derivation of all of these continuum models for fully and partially saturated media, the individual phases are usually mixed and their properties are averaged in a so-called representative elementary volume. During this averaging the individual interfaces between the wetting and non-wetting fluids in a pore disappear and the restoring force caused by the surface tension is not included in the continuum models for wave propagation in partially saturated rocks. Therefore, in these continuum models only the flow of the pore fluids caused by fluid pressure differences (described most frequently by Darcy flow) is considered. Additionally, numerical studies of microscale wave propagation in porous rocks (Saenger *et al.* 2007) also do not include surface tension effects. However, they include microscale scattering because they resolve the 3-D pore geometry.

In this study a basic 1-D model is presented that couples oscillations within a rock with the seismic wave propagation through the rock. The model is not intended to be an extension of the well-known Biot's equations (Biot 1962) to three phases (i.e. solid, wetting and non-wetting fluid), but rather to study the fundamental energy transfer between waves and oscillations and the resulting modification of the spectral content of elastic waves while propagating through a solid exhibiting internal oscillations. Here, oscillations caused by partial saturation of porous solids with a non-wetting fluid are considered. The remaining pore space is assumed to be filled by a gas. Resonance frequencies of such oscillations lie at the low-frequency end of the seismic spectrum (Hilpert 2007; Holzner *et al.* 2009). The motivation of this work is to couple the microscale pore fluid oscillation models (assuming a rigid elastic skeleton) to the macroscale elastic wave propagation model for the elastic skeleton. However, the model could be modified to study other oscillatory processes.

The paper starts by deriving the coupled wave propagation–oscillation model. Next, the resulting system of two coupled differential equations is solved numerically with explicit finite differences. The dispersion relation and the energy balance of the coupled system are studied numerically and analytically. Also, the spectral modification of elastic waves propagating through solids exhibiting internal oscillations is analysed. A discussion on the model's applicability to hydrocarbon reservoirs is followed by conclusions.

2 MATHEMATICAL MODEL

2.1 Elastic solid

The behaviour of the elastic solid in 1-D is described by the total stress in the elastic solid σ^{s}, the strain ε^{s}, being the spatial derivative of solid displacement u^{s} and the elastic modulus K. The elastic stress–strain constitutive relationship with x as the spatial coordinate is

$$\sigma^{\mathrm{s}} = K\varepsilon^{\mathrm{s}} = K\frac{\partial u^{\mathrm{s}}}{\partial x}, \tag{1}$$

where K represents the bulk modulus of the poroelastic rock, which is saturated by two immiscible fluids. The value of K is a function of the dry rock frame bulk modulus, the grain bulk modulus, the bulk moduli of the two fluids and the porosity (Gassmann 1951; Berryman & Milton 1991; Toms *et al.* 2006). There exists good understanding on the value of K within the general theory of porous media (Borja 2006; Gray & Schrefler 2007), and values of K are, for example, applied in the theory of wave propagation in partially saturated rocks (Santos *et al.* 1990; Tuncay & Corapcioglu 1996). In the low-frequency range, the Gassmann–Wood limit can be applied to estimate the value of K (Mavko *et al.* 1998). Thereby, Wood's law is used to calculate the effective fluid bulk modulus from the bulk moduli of the two immiscible fluids and this effective fluid bulk modulus is then used in the Gassmann relations (Gassmann 1951) to estimate the effective bulk modulus of the fluid saturated rock.

2.2 Fluid movement as linear oscillations

In the following, oscillations caused by partial saturation of porous solids with a non-wetting fluid are considered. The remaining pore space is assumed to be filled by a gas. Beresnev 2006 showed that the movement of such non-wetting fluids can be described with an oscillator equation. Here, a 1-D harmonic oscillator equation with an angular resonance frequency ω_0 is assumed to represent this oscillatory behaviour:

$$\ddot{u}^{\mathrm{f}} = -\omega_0^2\left(u^{\mathrm{f}} - u^{\mathrm{s}}\right). \tag{2}$$

Superscripts f and s refer to the non-wetting fluid and the solid rock frame, respectively, and u and $\ddot{u}$ are displacement and second time derivative of displacement. The restoring force that leads to a oscillatory behaviour is the surface tension force or capillary force (Dvorkin *et al.* 1990; Hilpert *et al.* 2000; Hilpert 2007; Holzner *et al.* 2009). Both the non-wetting pore fluid and the solid rock frame can be deformed, but only the relative displacement leads to a restoring force. Therefore, the relative displacement is used on the right-hand side of eq. (2). Hilpert *et al.* 2000 and Holzner *et al.* 2009 derived analytical formulae for ω_0 using different pore geometries and different boundary conditions at the pore wall. Hilpert *et al.* 2000 used a fluid blob with pinned contact lines in a pore with straight walls. The resulting formula is

$$\omega_0 = \sqrt{\frac{4\gamma}{r^2 h\rho^{\mathrm{f}}}\sin\theta_0\,(1+\sin\theta_0)^2}. \tag{3}$$

Holzner *et al.* 2009 used a fluid blob with sliding contact lines in a bi-conically shaped pore. The resulting formula is

$$\omega_0 = \sqrt{\frac{6\gamma}{rh^2\rho^{\mathrm{f}}}}. \tag{4}$$

In both formulae, the parameters γ, r, h and ρ^{f} are surface tension, radius of the pore, length of the fluid blob and density of the fluid, respectively. θ_0 in eq. (3) is the contact angle between the non-wetting fluid surface and the rigid pore wall. The two formulae have the same structure. Table 1 lists a set of parameters that is in accordance with the parameters used by Hilpert *et al.* 2000 and Holzner *et al.* 2009. Using these parameters, eq. (3) results in $\omega_0 = 107.7$ ($= 17.1$ Hz $\times\, 2\pi$) and eq. (4) in $\omega_0 = 75.1$ (=12.0 Hz $\times\, 2\pi$), which is the same order of magnitude. The difference is a result of the different pore geometries and boundary conditions at the pore walls of the two cases. Considering n oscillators, the total kinetic energy of the fluid $E^{\mathrm{f}}_{\mathrm{kin}}$ is

$$E^{\mathrm{f}}_{\mathrm{kin}} = \frac{1}{2}\sum_{j=1}^{n} m^{\mathrm{f}}_j\left(\dot{u}^{\mathrm{f}}_j\right)^2. \tag{5}$$

Table 1. Parameters used to calculate the resonance frequency ω_0 with eqs (3) and (4).

Parameter	Symbol	Value
Surface tension	γ	0.02 N m^{-1}
Radius of pore	r	0.001 m
Length of pore	h	0.005 m
Density of fluid	ρ^{f}	850 kg m^{-3}
Contact angle	θ_0	20°

In eq. (5) m_j^{f} and $\dot{u}_j^{\mathrm{f}}$ are mass and time derivative of the displacement of each individual oscillator. The pores are assumed to be non-connected. The individual oscillations therefore do not interact with each other directly. However, the individual fluid oscillations are coupled indirectly through their coupling to the solid (see below). Also, the individual oscillations are assumed to exhibit the same resonance frequency ω_0. These two major assumptions lead to a simplified model where no fluid flow between pores can take place. There will be no wave travelling due to the presence of the fluid, such as the Biot slow wave. However, the resulting model allows studying first-order effects of the oscillations on seismic wave propagation, which is included below. The total potential energy of the pore fluid, $E_{\mathrm{pot}}^{\mathrm{f}}$, is the sum of the individual potential energies:

$$E_{\mathrm{pot}}^{\mathrm{f}} = \frac{1}{2}\sum_{j=1}^{n} m_j^{\mathrm{f}}\omega_0^2\left(u_j^{\mathrm{f}} - u_j^{\mathrm{s}}\right)^2. \tag{6}$$

2.3 Coupling between fluid oscillations and elastic waves

The coupling of the microscale (i.e. pore-scale) fluid oscillations with a 1-D linear elastic solid yields the effective rheological model sketched in Fig. 1. Two displacements have to be considered individually in this model, the displacement of the solid phase u^{s} and the displacement of the oscillating fluid phase u^{f}. The solid is represented by a linear elastic element and the fluid by an oscillating mass. The elastic wave propagation and the fluid oscillations are coupled using Hamilton's variational principle for continuous systems (Fetter & Walecka 1980; Bourbie *et al.* 1987). Therefore, the energies of the oscillating fluid (eqs 5 and 6), which were defined in a discrete way, need to be reformulated in the continuous limit. The different contributions to the total system energy are then written in the following way:

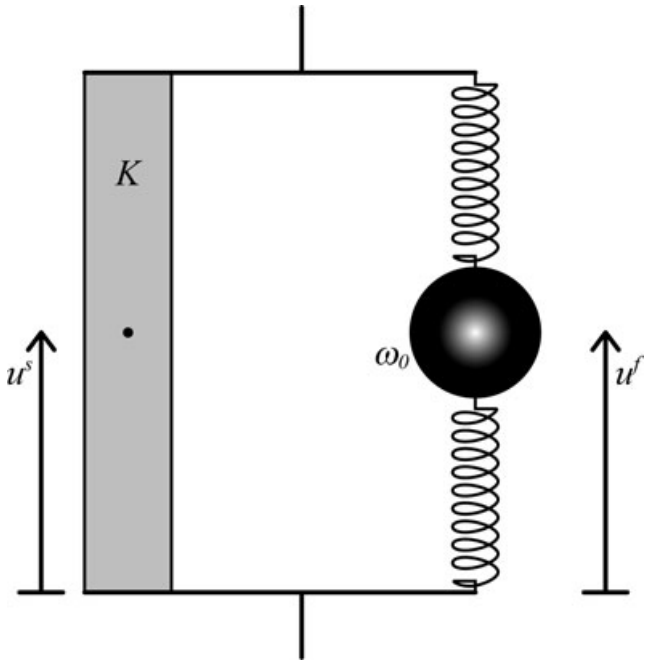

Figure 1. Schematic rheological model for coupling between elastic deformation and fluid oscillations. The elastic bar with bulk modulus K on the left-hand side is coupled in parallel with a linear oscillator with a resonance frequency ω_0.

$$E_{\mathrm{kin}}^{\mathrm{f}} = \frac{1}{2}\int_0^l S\phi\rho^{\mathrm{f}}\left(\dot{u}^{\mathrm{f}}\right)^2 \mathrm{d}x, \tag{7}$$

$$E_{\mathrm{pot}}^{\mathrm{f}} = \frac{1}{2}\int_0^l S\phi\rho^{\mathrm{f}}\omega_0^2\left(u^{\mathrm{f}} - u^{\mathrm{s}}\right)^2 \mathrm{d}x, \tag{8}$$

$$E_{\mathrm{kin}}^{\mathrm{s}} = \frac{1}{2}\int_0^l (1-\phi)\,\rho^{\mathrm{s}}\,(\dot{u}^{\mathrm{s}})^2\,\mathrm{d}x, \tag{9}$$

$$E_{\mathrm{pot}}^{\mathrm{s}} = \frac{1}{2}\int_0^l \sigma^{\mathrm{s}}\varepsilon^{\mathrm{s}}\mathrm{d}x. \tag{10}$$

Parameters ρ^{f}, ρ^{s} and l are density of the fluid and the solid, respectively, and length of the 1-D model. Parameters ϕ and S are porosity of the rock matrix and saturation of the pores by the non-wetting fluid, respectively. Both parameters are dimensionless and have a value between 0 and 1. They are both assumed to be constant in time, that is, porosity and saturation do not change when a wave is passing. Eqs (7)–(10) only consider the solid and the non-wetting fluid phase. In the presented cases, saturation of the pores is smaller than 1 and a third phase is present. It is assumed that the third phase is gaseous and that both its kinetic and potential energies are small compared to the fluid and solid phases. Therefore, the third phase is neglected. Also, the gaseous phase is assumed to have a much smaller bulk modulus than the fluid phase. Therefore, the compression of the fluid can be neglected and the fluid bulk modulus is not considered as a model parameter. Combining eqs (7)–(10), the Lagrangian functional L can be formulated (Fetter & Walecka 1980) using the total kinetic energy T and the total potential energy U:

$$L = T - U = \left(E_{\mathrm{kin}}^{\mathrm{f}} + E_{\mathrm{kin}}^{\mathrm{s}}\right) - \left(E_{\mathrm{pot}}^{\mathrm{f}} + E_{\mathrm{pot}}^{\mathrm{s}}\right) = \int_0^l \mathcal{L}\mathrm{d}x. \tag{11}$$

The Lagrangian density $\mathcal{L}$ has the dimension of energy per unit length. Hamilton's variational principle for continuous systems (Fetter & Walecka 1980; Bourbie *et al.* 1987) can now be applied to the Lagrangian functional:

$$\delta\int_{t_1}^{t_2} L\mathrm{d}t = \int_{t_1}^{t_2}\int_0^l \delta\mathcal{L}\mathrm{d}x\,\mathrm{d}t = \int_{t_1}^{t_2}\int_0^l \left\{\frac{\partial\mathcal{L}}{\partial u^{\mathrm{i}}} - \frac{\mathrm{d}}{\mathrm{d}t}\left(\frac{\partial\mathcal{L}}{\partial\dot{u}^{\mathrm{i}}}\right) - \frac{\mathrm{d}}{\mathrm{d}x}\left(\frac{\partial\mathcal{L}}{\partial\varepsilon^{\mathrm{i}}}\right)\right\}\delta u^i\,\mathrm{d}x\,\mathrm{d}t = 0. \tag{12}$$

Superscript i in eq. (12) replaces superscripts s (solid) or f (fluid). The variations δu^i are arbitrary (Fetter & Walecka 1980). Therefore, their coefficients in curly brackets must be equal to zero. The resulting equations are the Euler–Lagrange equations for the continuous two-component system:

$$\frac{\partial\mathcal{L}}{\partial u^{\mathrm{i}}} - \frac{\mathrm{d}}{\mathrm{d}t}\left(\frac{\partial\mathcal{L}}{\partial\dot{u}^{\mathrm{i}}}\right) - \frac{\mathrm{d}}{\mathrm{d}x}\left(\frac{\partial\mathcal{L}}{\partial\varepsilon^{\mathrm{i}}}\right) = 0. \tag{13}$$

The Lagrangian density $\mathcal{L}$ (in eq. 11) is substituted into the Euler–Lagrange equations. The final equations of motions are

$$S\phi\rho^{\mathrm{f}}\ddot{u}^{\mathrm{f}} = -S\phi\rho^{\mathrm{f}}\omega_0^2\left(u^{\mathrm{f}} - u^{\mathrm{s}}\right), \tag{14}$$

$$(1-\phi)\,\rho^{\mathrm{s}}\ddot{u}^{\mathrm{s}} = \frac{\partial}{\partial x}\left(K\frac{\partial u^{\mathrm{s}}}{\partial x}\right) + S\phi\rho^{\mathrm{f}}\omega_0^2\left(u^{\mathrm{f}} - u^{\mathrm{s}}\right). \tag{15}$$

Eqs (14) and (15) form a closed system of two equations for the two unknown functions u^{s} and u^{f}. eq. (14) is identical to a linear 1-D oscillator equation (eq. 2) but is formulated in terms of averaged density ($S\phi\rho^{\mathrm{f}}$). The left-hand side together with the first term of the right-hand side of eq. (15) represents a 1-D wave equation (Lindsay 1960; Achenbach 1973; Szabo 1985). It is also written in terms of averaged density [$(1–\phi)\rho^{\mathrm{s}}$]. This 1-D wave equation can represent a *P* wave or an *S* wave, depending on the interpretation of the unknown solid displacement u^{s} and the material parameter K. In this study, the solid displacement is assumed to be parallel to the propagation direction of the wave as well as parallel to the fluid displacement u^{f}. Therefore, in the following, the solid wave is called a *P* wave. The additional term on the right-hand side of eq. (15) links the fluid motion and the solid motion. If eqs (14) and (15) are added the coupling term disappears and the equation of conservation of the total linear momentum can be derived.

3 NUMERICAL MODEL

Eq. (1), the two eqs (14) and (15) and two additional kinematic equations ($\partial u^{\mathrm{i}}/\partial t = v^{\mathrm{i}}$) represent a coupled system of five first-order linear partial differential equations. The equations are spatially discretized over the model length l using the finite difference method with a 1-D staggered grid (Virieux 1986). The two displacements and the two velocities are defined on nodal points and the solid stress is defined on staggered points (i.e. centre points). Discretization in time is formulated explicitly with a staggered method (Virieux 1986). For some simulations the boundary conditions are rigid (all displacements and velocities are equal to zero) and for some simulations, non-reflecting (Ionescu & Igel 2003). Fig. 2 shows the model setup used in this study. Time signals are recorded at two synthetic receiver locations R_1 and R_2. For some simulations an external source is applied at the position S. In fact, the source is active over a small number of spatial gridpoints whereas the source amplitude is highest at position S and decays strongly over a few numerical points. The source acts as an additional force term in eq. (15) and therefore acts only on the elastic solid. The fluid phase is only affected indirectly through the coupling terms in eqs (14) and (15). The resonance frequency of the pore fluid oscillations is set to 3 Hz throughout the model domain but, using non-dimensionalization, the results can be translated to other frequencies. Physical parameters used in the simulations are given in Table 2. For all simulations the spatial resolution is chosen in such a way that the wavelength of a *P* wave with a frequency of 50 Hz is resolved with 50 nodal points. The explicit time increment is calculated using the von Neumann stability criterion (Virieux 1986; Higham 1996).

4 NUMERICAL RESULTS

4.1 Energy conservation and transfer

To test for conservation of energy of the numerical scheme a homogeneous numerical simulation was performed with two rigid boundaries (Fig. 2). No source function was applied, but a Gaussian-shaped initial perturbation of the solid velocity field was prescribed. After the simulation started, this perturbation propagates through the solid part of the model as an elastic wave and also initiates the fluid oscillations. In Fig. 3 the four energies in the system (eqs 7–10), which are calculated from the numerical simulation, are plotted versus time. The energies of the solid and the fluid phase always add up to a constant total system energy. The total energy of the system is conserved, which also illustrates the correctness of the numerical algorithm. At time zero, following the initial conditions, energy of the fluid is zero and energy of the solid is maximal. A significant part of the energy is then transferred back and forth between solid

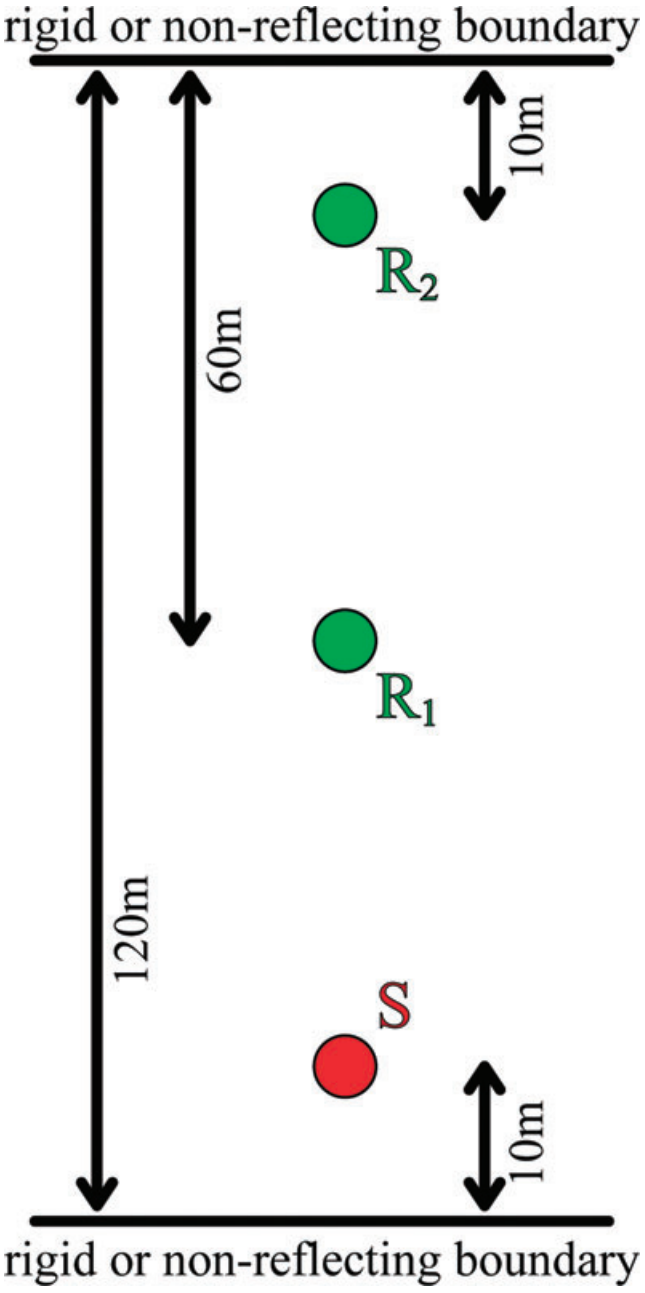

Figure 2. 1-D model setup for numerical simulations consists of two receivers R_1 and R_2 and one source S. The whole domain is described by the coupled system of eqs (14) and (15). The lower and upper boundaries can be rigid (zero displacement) or non-reflecting.

Table 2. Parameters used in numerical simulations.

Parameter	Symbol	Value
Resonance frequency of oscillations	ω_0	18.85 (= 3 Hz × 2π)
Density of fluid	ρ^{f}	800 kg m^{-3}
Density of solid	ρ^{s}	2800 kg m^{-3}
Elastic bulk modulus	K	10^{10}Pa
Porosity	ϕ	0.3
Non-wetting fluid saturation of pores	S	0.9
Frequency of external source	Ω	ω_0 / 10
High-frequency limit of P-wave velocity	V_P^{HF}	2259 m s^{-1}
Low-frequency limit of P-wave velocity	V_P^{LF}	2132 m s^{-1}

and fluid phase, showing that the pore fluid oscillations influence the behaviour of the solid phase considerably. For example, after about 0.4 s, the solid has transferred about 45 per cent of its total energy to the fluid (Fig. 3).

4.2 Eigenvalues and dispersion curve

In Fig. 4 the phase velocity dispersion curve for a P wave travelling in a medium described by the coupled eqs (14) and (15) is plotted. The black line is the analytical P-wave phase velocity as a function of frequency that is calculated from the eigenvalues of eqs (14) and (15). For calculating the phase velocity numerically (red dots in Fig. 4), several simulations were performed using different frequencies Ω in the external source function,

$$F(t) = \sin(\Omega t). \tag{16}$$

The source function was applied at position S of the model shown in Fig. 2 with two non-reflecting boundaries. The phase velocity of the P wave was calculated from the time-shift between the recordings at receivers R_1 and R_2. Numerical results agree well with the analytically calculated phase velocity and the numerical simulations reproduce well the phase velocity discontinuity around the resonance frequency.

The P-wave velocity in a dry poroelastic solid $\{\sqrt{K/[(1-\phi)\rho^{\mathrm{s}}]}\}$ is the high-frequency limit of the dispersion relation. At frequencies much larger than the resonance frequency, inertia prohibits a movement of the pore fluid and the seismic waves travel as if there was no pore fluid. At frequencies much smaller than the resonance frequency, solid and fluid move in phase. In this regime, the effective density that has to be considered in calculating the P-wave velocity is a combination of fluid and solid densities, and it becomes $\sqrt{K/[(1-\phi)\rho^{\mathrm{s}} + S\phi\rho^{\mathrm{f}}]}$. This low-frequency limit is very similar to the low-frequency limit of the Biot's equations (Gassmann 1951; Geerstma & Smit 1961) but using a constant bulk modulus. At frequencies just below the resonance frequency of the fluid oscillations a decrease of phase velocity is observed, followed by a sharp velocity jump at the resonance frequency to very high values. Mathematically, the phase velocity is indefinite at this point. With increasing frequencies the phase velocity decreases and finally reaches the high-frequency limit. This characteristic P-wave velocity dispersion curve is also observed in other media that exhibit an internal resonance behaviour. For example Fox *et al.* 1955, Silberman 1957 and Anderson & Hampton 1980a measured and described a very similar dispersion relation in water containing gas bubbles. Although the mechanism of oscillation is different, the effect on the propagation of seismic waves is comparable. The model described by eqs (14) and (15) conserves energy (Fig. 3). Therefore, P waves are not attenuated. Attenuation can be calculated from the eigenvalues of the system of eqs (14) and (15), but it results in zero attenuation for all frequencies.

4.3 Spectrograms for wave incidence

A numerical simulation was run with the model setup shown in Fig. 2 with two non-reflecting boundaries. The external source applied at position S is a Gaussian curve in time,

$$F(t) = \exp\left[-\frac{(t-t_0)^2}{2\tau^2}\right], \tag{17}$$

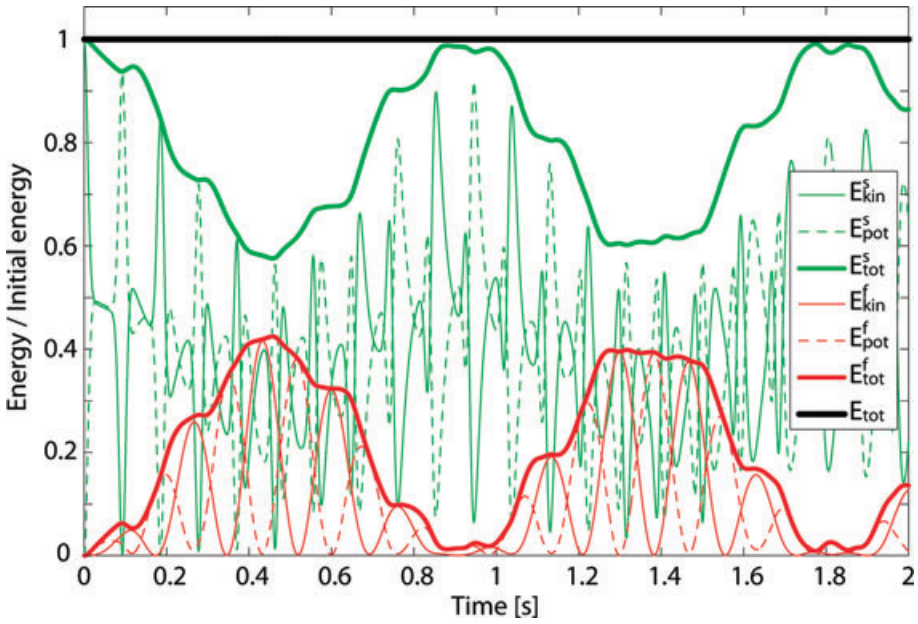

Figure 3. Time evolution of the different energies in the coupled system (eqs 7–10). A 120 m long homogeneous model with two rigid boundaries is used, and an initial perturbation in the solid velocity field is applied. The total energy, that is, the sum of all energies (thick black line) stays constant over time. Individual energy contributions are transferred between fluid (red lines) and solid (green lines) phases.

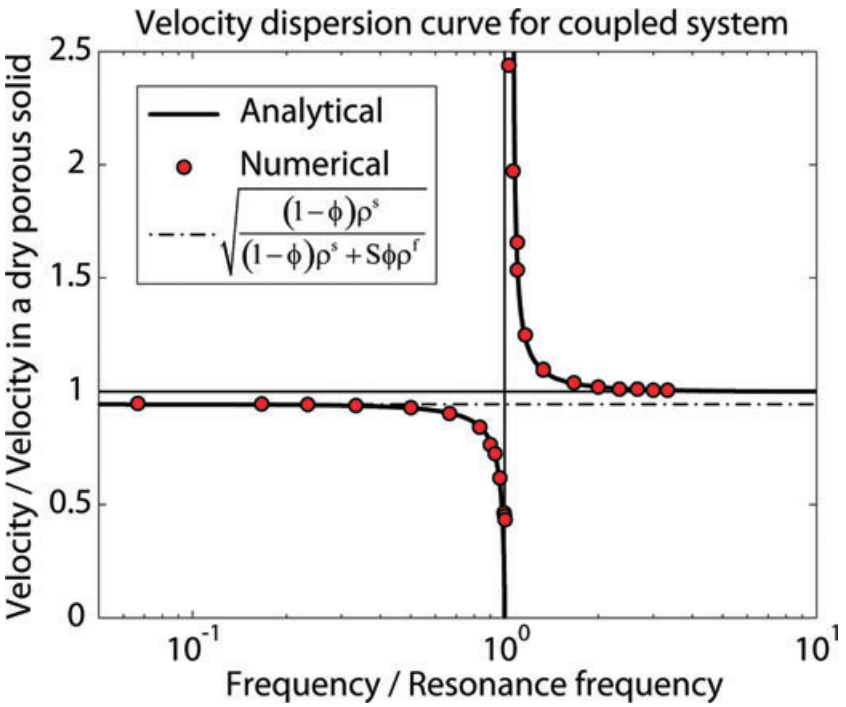

Figure 4. *P*-wave phase velocity versus frequency. Frequency is normalized with the resonance frequency of the fluid oscillations. Velocity is normalized with the phase velocity in a dry porous rock. Analytical phase velocity is calculated from the eigenvalues of the system of eqs (14) and (15). Numerical phase velocities are calculated from simulations with a monochromatic external source. Each point represents one individual simulation using one particular external frequency.

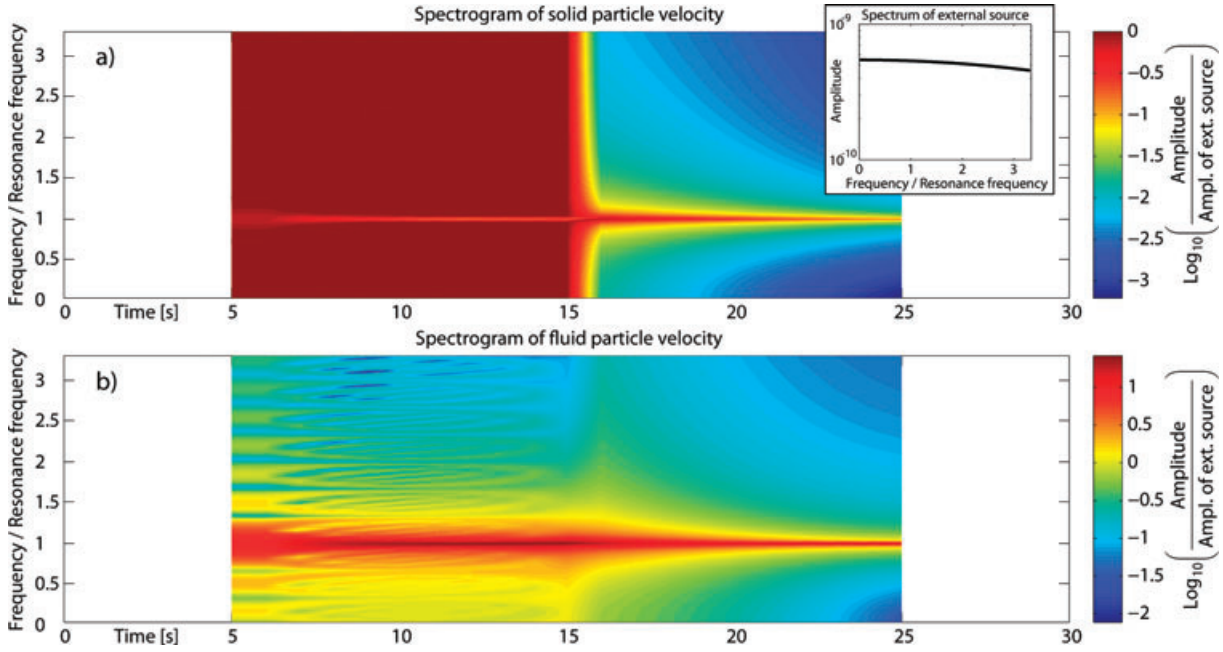

Figure 5. Spectrogram of solid (a) and fluid (b) particle velocities at receiver R_2 of the model shown in Fig. 2, with two non-reflecting boundaries. Inlay: Spectrum of the applied Gaussian source function (eq. 17) applied at position S. Frequency is normalized with the resonance frequency of the fluid oscillations. Spectral values are normalized with the spectrum of the source function and are plotted logarithmically. Due to the algorithm calculating the spectrograms (see text), the Gaussian peak of the external source is visible for 10 s (between 5 and 15 s).

where $t_0 = 10$ s and $\tau = 0.01$ s. The inlay in Fig. 5(a) shows the spectrum of this source function. At receiver R_2, both fluid and solid particle velocities were recorded. Fig. 5 shows the spectrograms for both particle velocities. The spectral values are normalized with the spectrum of the external source. To calculate a spectrogram, a 10 s time window is moved along the time axis of the recorded particle velocity–time signal with 1 s steps. For each step, the spectrum is calculated and plotted at the centre of the 10 s window. Due to this algorithm, the pulse of the external source is visible in the spectrogram between 5 and 15 s. Over this time interval, the

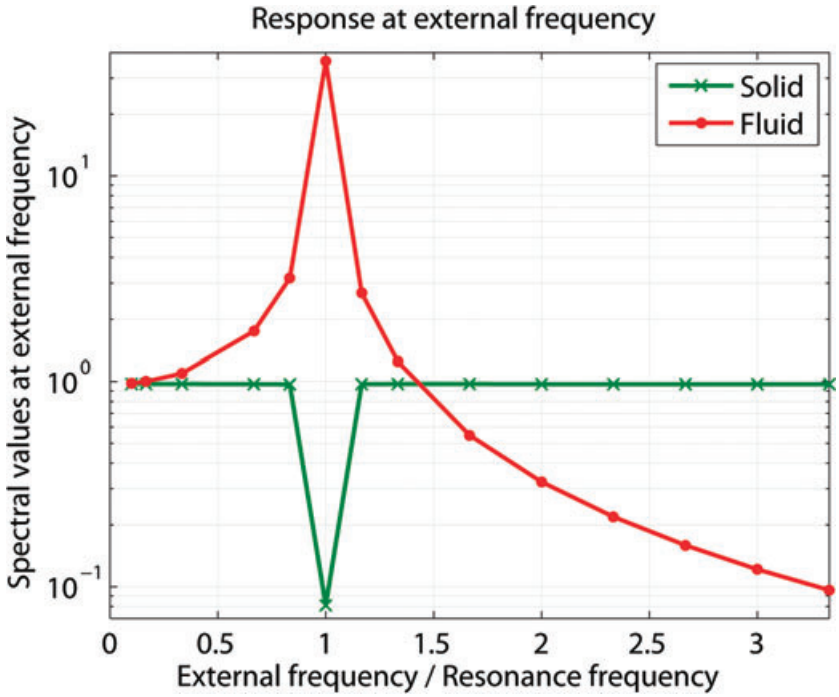

Figure 6. Spectral response of the fluid and solid particle velocity at the external source frequency for different external frequencies. Velocities are recorded at receiver R_2 of the model shown in Fig. 2, with two non-reflecting boundaries. One simulation with a monochromatic source function (eq. 16) at position S provides the two data points at one frequency. Frequency is normalized with the resonance frequency of the fluid oscillations. Spectral values are normalized with the spectral values of the external source.

spectrogram of the solid particle velocity (Fig. 5a) shows a minimum at the resonance frequency of the fluid oscillations. The amplitude of this minimum is around one order of magnitude smaller than the amplitude of the external source (orange colour of the minimum). The second half of the spectrogram, where the external source is not present, shows a peak at this frequency. Immediately after the source pulse has passed, this peak has the same amplitude as the source at this frequency (dark red colour of the peak). The amplitude of the peak decreases over time, becoming around one order of magnitude smaller after 25 s (orange colour). The spectrogram of the fluid velocity (Fig. 5b) shows a peak at the resonance frequency of the fluid oscillations throughout the whole simulation. The amplitude of this peak is larger than the amplitude of the external source at this frequency.

Fig. 5 indicates that at the moment of incidence of the elastic wave, fluid oscillations are immediately excited. The oscillations take place at the resonance frequency. Therefore, a maximum at the resonance frequency develops in the spectrogram of the fluid particle velocity from the very beginning of the simulation (Fig. 5b). At the same time, a minimum in the spectrogram of the solid particle velocity develops at this frequency (Fig. 5a). This happens because the energy for the initiation of the fluid oscillations is taken from the solid. This energy transfer from solid to fluid takes place only at the resonance frequency due to the linear nature of the system equations. After the fluid oscillations are initiated and the elastic wave has passed, the fluid continues to oscillate with its resonance frequency. Fluid oscillations in adjacent pores are almost in phase because they are excited by the macroscale elastic wave at almost the same instant. Therefore, the effect of the different pores on the seismic wave adds up to a measurable effect. The oscillating fluid continuously transfers energy back to the solid. This energy transfer from fluid to solid happens only at the resonance frequency due to the linear nature of the system equations. Therefore, a maximum in the spectrogram of the solid particle velocity occurs at this frequency (Fig. 5a). The amplitude of this peak cannot be larger than the amplitude of the external source, which initialized the oscillations. The non-reflecting boundaries of the system allow the *P*-waves to transport energy out of the system. Therefore, the fluid oscillations decrease in amplitude and the maxima in both spectrograms decrease.

4.4 Resonance curves

Fig. 6 shows two resonance curves for the coupled eqs (14) and (15). The two curves represent the solid and the fluid response at the frequency of the external source. They are numerically calculated in the following way: a set of numerical simulations was performed using a different frequency Ω in the monochromatic external source function (eq. 16) for each of the simulations. The source function was applied at position S of the model shown in Fig. 2 with two non-reflecting boundaries. For each simulation two mean spectra are calculated, one for the fluid particle velocity and one for the solid particle velocity, both recorded for 300 s at receiver R_2. Mean spectra are calculated by arithmetically averaging in time the spectrograms that are calculated the same way as described above for Fig. 5. From these two mean spectra, the spectral values are picked at the external frequency Ω. Each simulation (i.e. each external frequency) results in two spectral values (i.e. solid and fluid response at the external frequency) that are plotted in Fig. 6. The frequency is normalized with the resonance frequency of the fluid oscillations. Spectral values are normalized with the spectral values of the external source function.

As expected for an oscillatory behaviour, the closer the external frequency is to the resonance frequency the stronger the fluid

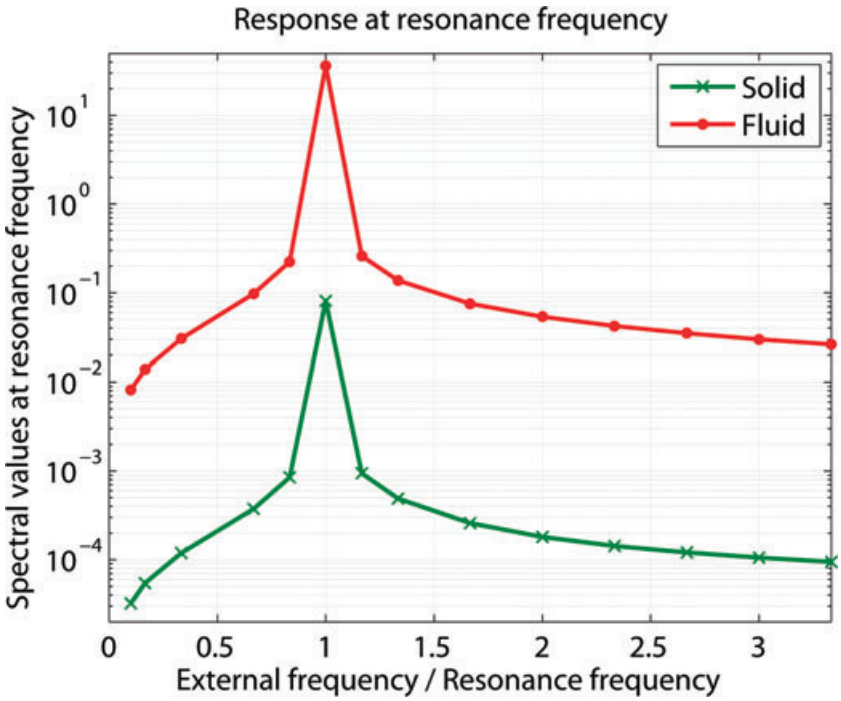

Figure 7. Spectral response of the fluid and solid particle velocity at the resonance frequency for different external frequencies. Velocities are recorded at receiver R_2 of the model shown in Fig. 2 with two non-reflecting boundaries. One simulation with a monochromatic source function (eq. 16) at position S provides the two data points at one frequency. Frequency is normalized with the resonance frequency of the fluid oscillations. Spectral values are normalized with the spectral values of the external source.

response becomes. Below the resonance frequency, the fluid response is equal to the solid response at very low external frequencies. Above the resonance frequency, the fluid response becomes much smaller than the solid response with increasing frequency. The solid response is equal to the external source for all frequencies except for a sharp minimum at the resonance frequency of the fluid oscillations. The amplitude of this minimum is around one order of magnitude smaller than the amplitude of the external source. This is very similar to the minimum described in the first half of Fig. 5(a). The observations in Fig. 6 can be interpreted with the energy transfer already described for Figs 3 and 5. The minimum in the solid response develops because energy is transferred from solid to fluid only at the resonance frequency to drive the fluid oscillations. At very low frequencies, the fluid moves in phase with the solid. Consequently, the fluid response at very low external frequencies is equal to the solid response. At very high external frequencies, inertia of the fluid prohibits excitation of the oscillations and the fluid does not move. Consequently, the fluid response becomes very small with increasing frequency.

Fig. 7 shows two resonance curves that are similar to the ones in Fig. 6. The two curves represent the solid and the fluid response at the resonance frequency of the fluid oscillations. They are calculated in the same way as described above for Fig. 6, but instead of picking the spectral values at the external frequency in the mean spectra, the spectral values are picked at the resonance frequency. Normalization of the frequency and of the spectral values is also done in the same way as in Fig. 6. The two data points at an external frequency equal to the resonance frequency are the same data points as in Fig. 6 at the same frequency. The two curves in Fig. 7 have the same shape but different amplitudes. They clearly represent the resonance effect of the fluid. The closer the external frequency is to the resonance frequency, the stronger the fluid response becomes. Because energy transfer between fluid and solid only takes place at the resonance frequency, the solid response at the resonance frequency is dominated by the oscillatory behaviour of the fluid. However, the fluid oscillations are also excited for other external frequencies than the resonance frequency, that is, spectra do not drop to zero for external frequencies different from the resonance frequency. This is an effect of the incidence of the elastic wave at the beginning of each simulation. At the moment of elastic wave incidence, all frequencies are introduced into the system and the fluid oscillations are excited. This excitation is stronger for elastic waves having a frequency close to the resonance frequency.

4.5 Comparison to purely elastic case

From the set of numerical simulations used in Figs 6 and 7, one simulation is taken for comparison with a purely elastic model. The chosen simulation uses a monochromatic external source (eq. 16) applied at position S with a frequency Ω, 10 times smaller than the resonance frequency. This choice is motivated by the fact that the Fourier spectra of typical passive measurements of seismic background noise show a dominant peak at around 0.2 Hz (Peterson 1993; Berger *et al.* 2004), which is about a factor 10 smaller than the applied resonance frequency. This high-energy spectral peak is a global feature that can be measured everywhere in the world and is presumably related to seismic surface waves generated by ocean waves (Aki & Richards 1980). After different simulation durations, a Fourier spectrum is calculated from the solid particle velocity recorded at receiver R_2. The procedure to calculate a spectrum is not a moving-window method with a constant time-window length but always uses the whole time signal from the beginning of the simulation until the current time. It is therefore different from the

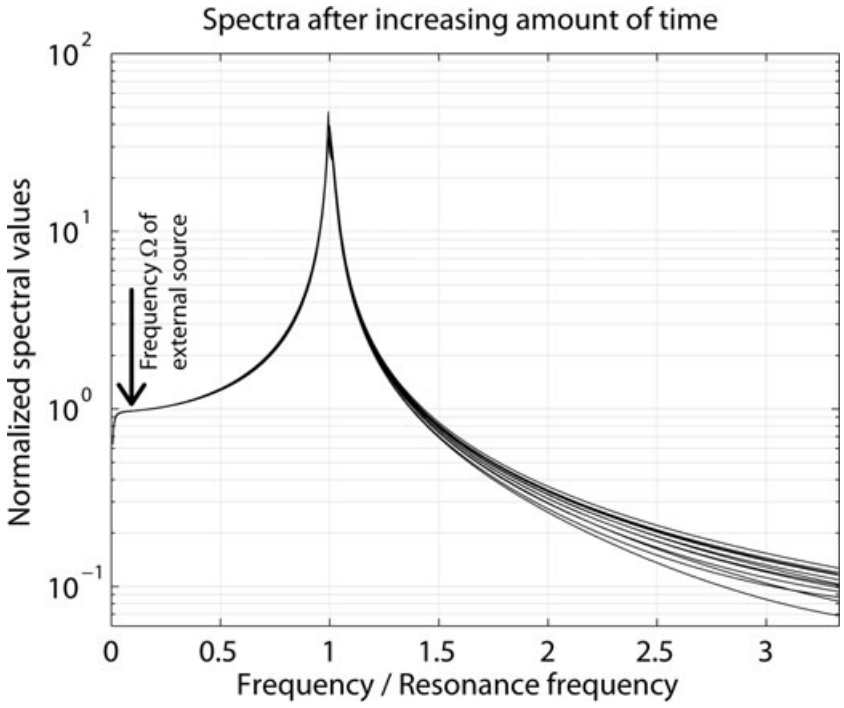

Figure 8. Fourier spectra of solid particle velocity–time signal at receiver R_2 of the model shown in Fig. 2 with two non-reflecting boundaries. A monochromatic source (eq. 16) is applied at position S with a frequency 10 times smaller than the resonance frequency of the fluid oscillations. Different spectra are calculated after different simulation lengths. Longest time signal is 120 s, shortest is 3.5 s. Frequency is normalized with the resonance frequency of the fluid oscillations. Spectra are normalized with spectra of the analytically calculated solid particle velocity–time signal at the same receiver but for a purely elastic model.

method used to produce Figs 5–7. For the same simulation duration, a model is considered that has the same dimensions, the same source and receiver locations and the same elastic properties as the numerical model but is purely elastic and does not exhibit internal oscillations. Because this additional model is purely elastic, the particle velocity–time signal at receiver R_2 can be analytically calculated.

Fig. 8 shows the division of the Fourier spectrum derived from the numerical simulation (model exhibiting internal oscillations) by the Fourier spectrum derived from the analytical time signal (purely elastic) for different simulation lengths. The frequency is normalized with the resonance frequency of the fluid oscillations. The two spectra before the division (not shown here) show a very distinct peak at the frequency of the external source. This peak has a constant value after different simulation durations. Also, this peak has the same value for both models (with internal oscillations and purely elastic) and therefore cancels to a value of 1 when the two spectra are divided (Fig. 8). Evolution of the two spectra before the division (not shown here) shows that the spectral amplitude of all other frequencies than the external frequency decreases with increasing simulation duration. This decrease of spectral amplitudes is exactly the same for the two cases (with internal oscillations and purely elastic). Therefore, the division of the two spectra lets them collapse onto one single curve (Fig. 8), no matter what simulation duration was considered.

The decrease of spectral amplitudes with increasing simulation duration before the spectral division is interpreted in the following way. The particle velocity–time signal contains the incidence of the elastic wave front as the first event. This event introduces all frequencies when the Fourier spectrum is calculated. After that, the particle velocity–time signal contains only the signal of the monochromatic source (in the purely elastic case) and the signal of the oscillating fluid that is transferred to the solid. For a long simulation, the monochromatic part of the time signal dominates and the first event, which introduced all other frequencies, becomes less important in calculating the Fourier spectrum. Therefore, although the monochromatic part of the time signal stays constant, the spectral amplitude of all other frequencies decreases with time. Fig. 8 therefore shows the time-independent spectral difference between the recorded particle velocity–time signal at receiver R_2 of the model exhibiting internal oscillations and the purely elastic model. The strong peak at the resonance frequency is initiated at the very beginning of the simulation when the wave front of the source signal propagates through the medium and initiates the fluid oscillations. The time-constant peak in Fig. 8 shows that the amplitude at the resonance frequency decreases with the same rate as in the purely elastic case and that no intrinsic attenuation due to the fluid oscillations takes place.

5 DISCUSSION

The oscillation behaviour of individual, partially saturated pores was studied thoroughly theoretically (Graham & Higdon 2000b), experimentally (Li *et al.* 2005) and numerically (Hilpert 2007; Pride *et al.* 2008; Holzner *et al.* 2009). However, the influence of such oscillations on the propagation of seismic waves in the porous skeleton was not studied in detail. Also, oscillatory behaviour of fluids and surface tension effects are not included in poroelastic theories, such as Biot Theory (Biot 1962), in patchy-saturation models (White 1975; White *et al.* 1975; Dutta & Ode 1979), in 3-phase wave propagation models (Santos *et al.* 1990; Lo & Sposito 2005), nor in microscale models of porous flow (Saenger *et al.* 2007). For studying fundamental effects of the coupling between fluid

oscillations and seismic wave propagation, the presented model equations (eqs 14 and 15) are intentionally kept simple. Additional effects, for example, damping of the oscillations, interaction between individual pores (i.e. connected pores), attenuation of seismic waves, non-linear oscillations due to more complex pore geometries or more spatial dimensions could be included to gain more insight into the coupling effects. Despite the simplicity of the model, the dispersion relation (Fig. 4) agrees well with the dispersion relation for water containing gas bubbles (Fox *et al.* 1955; Silberman 1957; Anderson & Hampton 1980a), which is a comparable problem of a wave travelling through a medium exhibiting internal oscillations.

Because the system eqs (14) and (15) are linear, the energy transfer between solid and fluid only happens at the resonance frequency of the oscillations (Figs 5a and 6). Therefore, the source, which is only active in the solid in the presented cases, needs to contain some energy at this frequency for the oscillations to be initiated. Even using a monochromatic source (eq. 16), every point in the model experiences a moment of seismic wave incidence because simulations are done in the time-domain. The wavefield is therefore not stationary like in a frequency-domain simulation. At the moment of seismic wave incidence all frequencies are introduced into the model, despite the monochromatic source, and the oscillations are initiated. After the wave front has passed, the fluid continues to oscillate and constantly transfers energy to the elastic porous matrix. This results in a decrease of amplitude of the oscillations as long as the oscillations stay undisturbed (Fig. 5a). Seismic background noise in nature (Aki & Richards 1980; Peterson 1993) contains the most energy at around 0.2 Hz but also at larger frequencies with smaller amplitudes. Additionally, natural wavefields show significant variations in amplitude. These amplitude variations can have similar effects as individual incident wave pulses, which can potentially drive the fluid oscillations.

A possible application of the coupled wave propagation–oscillation model presented here is passive low-frequency spectral analysis applied for detection of hydrocarbon reservoirs (Dangel *et al.* 2003; Graf *et al.* 2007; Walker 2008; Lambert *et al.* 2008; Holzner *et al.* 2009). Passive low-frequency measurements show increased spectral amplitudes between 1 to 6 Hz when the ambient seismic background noise is measured above a hydrocarbon reservoir compared with measurements in areas without a reservoir. Several different physical mechanisms are discussed as a potential cause of this phenomenon (Graf *et al.* 2007), but no accepted physical theory has been published until now. Current models suggest that reservoirs act like a filter or scatterer and modify the ambient seismic background noise. Fluid oscillations and surface tension effects could play an important role in hydrocarbon reservoirs because of the coexistence of a wetting and a non-wetting phase in the pores and other cavities, such as fractures. The presented model requires that the ambient seismic background noise contains some energy at the resonance frequency of the oscillations (presumably between 1 and 6 Hz) at reservoir depth. Bradley *et al.* 1997 and Bonnefoy-Claudet *et al.* 2006 indicate that the spectral amplitude of the ocean wave peak (0.2 Hz) stays very constant with depth but that spectral amplitudes of higher frequencies drop relatively fast with depth. However, ambient seismic noise still contains energy at these higher frequencies at reservoir depth. The presented model also requires a partial saturation of the pore space. A hydrocarbon reservoir can be only partially saturated or fully saturated. However, the effect in nature is expected to be stronger close to the oil–water contact, close to the oil–gas contact or at the margin of a reservoir, where the pores are partially saturated.

In natural environments, the resonance frequency of the fluid oscillations is not expected to be constant for all pores due to complex pore geometries, different pore sizes, different degree of connectivity or different degree of saturation. In addition, there can be other effects causing oscillatory behaviour of a solid with a different resonance frequency, such as multiple reflections in layered media (Urquizu & Correig 2004) or resonant scattering at heterogeneities (Werby & Gaunaurd 1989; Werby & Gaunaurd 1990; Hassan & Nagy 1997). Therefore, natural media should be represented by a range of resonance frequencies rather than one particular value. The expected effects are smoother peaks and minima rather than such strong and distinct peaks and minima shown in Figs 5–8.

6 CONCLUSIONS

The impact of media exhibiting internal oscillations on elastic waves propagating through such media is studied with a basic 1-D model that couples microscale oscillations with macroscale seismic waves. Oscillations are assumed to arise from non-wetting fluids trapped in pores or other cavities in the solid rock matrix but can also arise from other processes. The coupling of fluid oscillations with wave propagation models causes dispersion of the *P*-wave velocities around the resonance frequency (Fig. 4). Numerical simulations show that incident seismic waves initiate oscillations in the media. The energy required for the initiation of the oscillations is transferred from solid to fluid at the resonance frequency. A seismic wave front therefore looses energy at the resonance frequency and a minimum in the spectrum of the solid particle velocity develops. After the wave front has passed, the fluid continues to oscillate with its resonance frequency and energy is continuously transferred back from fluid to solid. Therefore, a peak develops in the spectrum of the solid particle velocity after the wave front has passed. The continuous transfer of energy from fluid to solid after the wave front has passed leads to a decrease of amplitude of the fluid oscillations. Consequently, the spectral peak at the resonance frequency also decreases with increasing time (Fig. 5). However, no intrinsic attenuation takes place due to the fluid oscillations (Fig. 8).

The results indicate that the frequency content of a wavefield can be modified by a medium exhibiting a resonance frequency as long as the original wavefield contains energy at the resonance frequency. Depending on the piece of the recorded particle velocity–time signal used for calculating the Fourier spectrum the spectral amplitude at the resonance frequency can be larger (i.e. a peak) or smaller (i.e. a minimum) than in the original wave. No constant peak or constant minimum is expected.

The presented model is a basic one for studying fundamental effects. It includes the impact of fluid oscillations on propagating waves that is not included in poroelastic theories or in microscale models. Oscillatory effects might play an important role in natural porous media that are partially saturated with a non-wetting fluid, such as hydrocarbon reservoirs, or other media exhibiting a resonance frequency. Despite the simplicity of the presented model, the dispersion relation agrees well with the one for water containing gas bubbles, which is another example of a medium exhibiting a resonance frequency.

ACKNOWLEDGMENTS

Many discussions with Reto Holzner and Holger Steeb are greatly acknowledged, as well as the help of Beatriz Quintal, Marc

Lambert and Brian Steiner. This work was supported by ETH Zurich, the Swiss Commission for Technology and Innovation (CTI) and Spectraseis AG.

REFERENCES

Achenbach, J.D., 1973. *Wave Propagation in Elastic Solids*, North-Holland Publishing Company, Amsterdam, ISBN 0–7204-2367–8.

Aki, K. & Richards, P.G., 1980. *Quantitative Seismology: Theory and Methods*, W. H. Freeman and Company, San Francisco, ISBN 0–7167-1058–7.

Anderson, A.L. & Hampton, L.D., 1980a. Acoustics of gas-bearing sediments, I: background, *J. acoust. Soc. Am.,* **67,** 1865–1889.

Anderson, A.L. & Hampton, L.D., 1980b. Acoustics of gas-bearing sediments, II: measurements and models, *J. acoust. Soc. Am.,* **67,** 1890–1903.

Beresnev, I.A., 2006. Theory of vibratory mobilization on nonwetting fluids entrapped in pore constrictions, *Geophysics,* **71,** N47–N56.

Beresnev, I.A. & Johnson, P.A., 1994. Elastic-wave stimulation of oil production: a review of methods and results, *Geophysics,* **59,** 1000–1017.

Beresnev, I.A., Vigil, R.D., Li, W., Pennington, W.D., Turpening, R.M., Iassonov, P.P. & Ewing, R.P., 2005. Elastic waves push organic fluids from reservoir rock, *Geophys. Res. Lett.,* **32,** L13303.

Berger, J., Davis, P. & Ekstrom, G., 2004. Ambient Earth noise: a survey of the Global Seismographic Network, *J. geophys. Res.(Solid Earth),* **109,** B11307.

Berryman, J.G. & Milton, G.W., 1991. Exact results for generalized Gassmann's equations in composite porous media with two constituents, *Geophysics,* **56,** 1950–1960.

Biot, M.A., 1962. Mechanics of deformation and acoustic propagation in porous media, *J. appl. Phys.,* **33,** 1482–1498.

Bonnefoy-Claudet, S., Cotton, F. & Bard, P.-Y., 2006. The nature of noise wavefield and its applications for site effects studies: a literature review, *Earth-Sci. Rev.,* **79,** 205–227.

Borja, R.I., 2006. On the mechanical energy and effective stress in saturated and unsaturated porous continua, *Int. J. Solids Struct.,* **43,** 1764–1786.

Bourbie, T., Coussy, O. & Zinszner, B., 1987. *Acoustics of Porous Media,* Editions Technip, Paris, ISBN 2–7108-0516–2.

Bradley, C.R., Stephen, R.A., Dorman, L.M. & Orcutt, J.A., 1997. Very low frequency (0.2–10.0 Hz) seismoacoustic noise below the seafloor, *J. geophys. Res. (Solid Earth),* **102,** 11 703–11 718.

Castellini, P., Esposito, E., Paone, N. & Tomasini, E.P., 2000. Non-invasive measurements of damage of frescoes paintings and icon by laser scanning vibrometer: experimental results on artificial samples and real works of art, *Measurement,* **28,** 33–45.

Dangel, S., Schaepman, M.E., Stoll, E.P., Carniel, R., Barzandji, O., Rode, E.-D. & Singer, J.M., 2003. Phenomenology of tremor-like signals observed over hydrocarbon reservoirs, *J. Volcanol. Geotherm. Res.,* **128,** 135–158.

Dutta, N.C. & Odé, H., 1979. Attenuation and dispersion of compressional waves in fluid-filled porous rocks with partial gas saturation (White model), Part I: Biot theory, *Geophysics,* **44,** 1777–1788.

Dvorkin, J., Mavko, G. & Nur, A., 1990. The oscillations of a viscous compressible fluid in an arbitrarily-shaped pore, *Mech. Mater.,* **9,** 165–179.

Fetter, A.L. & Walecka, J.D., 1980. *Theoretical Mechanics of Particles and Continua,* McGraw-Hill Book Company, New York, ISBN 0–07-020658–9.

Fox, F.E., Curley, S.R. & Larson, G.S., 1955. Phase velocity and absorption measurements in water containing air bubbles, *J. acoust. Soc. Am.,* **27,** 534–539.

Frehner, M., Schmalholz, S.M., Saenger, E.H. & Steeb, H., 2008. Comparison of finite difference and finite element methods for simulating two-dimensional scattering of elastic waves, *Phys. Earth planet. Inter.,* **171,** 112–121.

Gassmann, F., 1951. Über die Elastizität poröser Medien, *Vierteljahrsschrift der Naturforschenden Gesellschaft Zürich,* **96,** 1–23.

Geerstma, J. & Smit, D.C., 1961. Some aspects of elastic wave propagation in fluid-saturated porous solids, *Geophysics,* **26,** 169–181.

Graf, R., Schmalholz, S.M., Podladchikov, Y. & Saenger, E., 2007. Passive low frequency spectral analysis: exploring a new field in Geophysics, *World Oil,* January, 47–52.

Graham, D.R. & Higdon, J.J.L., 2000a. Oscillatory flow of droplets in capillary tubes, Part 1: straight tubes, *J. Fluid Mech.,* **425,** 31–53.

Graham, D.R. & Higdon, J.J.L., 2000b. Oscillatory flow of droplets in capillary tubes, Part 2: constricted tubes, *J. Fluid Mech.,* **425,** 55–77.

Gray, W.G. & Schrefler, B.A., 2007. Analysis of the solid phase stress tensor in multiphase porous media, *Int. J. Numer. Anal. Meth. Geomech.,* **31,** 541–581.

Hassan, W. & Nagy, P.B., 1997. Circumferential creeping waves around a fluid-filled cylindrical cavity in an elastic medium, *J. acoust. Soc. Am.,* **101,** 2496–2503.

Higham, N.J., 1996. *Accuracy and Stability of Numerical Algorithms,* Society for Industrial & Applied Mathematics, Philadelphia, ISBN 0–89871-355–2.

Hilpert, M., 2007. Capillarity-induced resonance of blobs in porous media: analytical solutions, Lattice-Boltzmann modeling, and blob mobilization, *J. Colloid Interface Sci.,* **309,** 493–504.

Hilpert, M., Jirka, G.H. & Plate, E.J., 2000. Capillarity-induced resonance of oil blobs in capillary tubes and porous media, *Geophysics,* **65,** 874–883.

Holzner, R., Eschle, P., Dangel, S., Frehner, M., Narayanan, C. & Lakehal, D., 2009. Hydrocarbon microtremors interpreted as nonlinear oscillations driven by oceanic background waves, *Commun. Nonlinear Sci. Numer. Simulat.,* **14,** 160–173.

Iassonov, P.P. & Beresnev, I.A., 2003. A model for enhanced fluid percolation in porous media by application of low-frequency elastic waves, *J. geophys. Res. (Solid Earth),* **108(B3),** 2138, doi:10.1029/2001JB000683.

Ida, N. & Wang, J.S., 1996. Models for microwave nondestructive testing of materials, *Materials Science Forum,* Vols. 210–213 (Non destructive Characterization of Materials VII), pp. 93–100.

Ionescu, D.-C. & Igel, H., 2003. Transparent boundary conditions for wave propagation on unbounded domains, in *Proceedings of the Computational Science—ICCS 2003, Part III,* pp. 807–816, Springer Verlag, Berlin, ISBN 978-3-540-40196-4.

Lambert, M.-A., Schmalholz, S.M. Saenger, E.H. & Steiner, B., 2008. Low-frequency microtremor anomalies at an oil and gas field in Voitsdorf, Austria, *Geophys. Prospect.,* in press, doi:10.1111/j.1365–2478.2008.00734.x.

Landau, L.D. & Lifschitz, E.M., 1997. *Mechanik,* Harri Deutsch Verlag, Thun, ISBN 3–8171-1326–9.

Li, W., Vigil, R.D., Beresnev, I.A., Iassonov, P. & Ewing, R., 2005. Vibration-induced mobilization of trapped oil ganglia in porous media: experimental validation of a capillary-physics mechanism, *J. Colloid Interface Sci.,* **289,** 193–199.

Lindsay, R.B., 1960. *Mechanical Radiation,* McGraw-Hill Book Company, New York, ISBN 00–703784-40.

Lo, W.-C. & Sposito, G., 2005. Wave propagation through elastic porous media containing two immiscible fluids, *Water Resource. Res.,* **41,** W02025.

Mavko, G., Mukerji, T. & Dvorkin, J., 1998. *The Rock Physics Handbook,* Cambridge University Press, Cambridge, ISBN 0–521-54344–4.

Meyer, E., Brendel, K. & Tamm, K., 1958. Pulsation oscillations of cavities in rubber, *J. acoust. Soc. Am.,* **30,** 1116–1124.

Peterson, J., 1993. Observations and modeling of seismic background noise, Open-File Report 93–322, U.S. Geological Survey, Albuquerque, New Mexico, USA.

Pride, S.R., Flekkøy, E.G. & Aursjø, O., 2008. Seismic stimulation for enhanced oil recovery, *Geophysics,* **73,** O23–O35.

Saenger, E.H., Ciz, R., Krüger, O.S., Schmalholz, S.M., Gurevich, B. & Shapiro, S.A., 2007. Finite-difference modeling of wave propagation on microscale: a snapshot of the work in progress, *Geophysics,* **72,** SM293–SM300.

Santos, J.E., Douglas, J., Corbero, J. & Lovera, O.M., 1990. A model for wave propagation in a porous medium saturated by a two-phase fluid, *J. acoust. Soc. Am.,* **87,** 1439–1448.

Schultz, T., Cattafesta, L.N. & Sheplak, M., 2006. Modal decomposition method for acoustic impedance testing in square ducts, *J. acoust. Soc. Am.,* **120,** 3750–3758.

Silberman, E., 1957. Sound velocity and attenuation in bubbly mixtures measured in standing wave tubes, *J. acoust. Soc. Am.,* **29,** 925–933.

Smeulders, D.M.J. & Van Dongen, M.E.H., 1997. Wave propagation in porous media containing a dilute gas-liquid mixture: theory and experiments, *J. Fluid Mech.,* **343,** 351–373.

Szabo, I., 1985. *Höhere Technische Mechanik,* Springer-Verlag, Berlin, ISBN 3–540-15007–2.

Toms, J., Müller, T.M., Ciz, R. & Gurevich, B., 2006. Comparative review of theoretical models for elastic wave attenuation and dispersion in partially saturated rocks, *Soil Dyn. Earthq. Eng.,* **26,** 548–565.

Tuncay, K. & Corapcioglu, M.Y., 1996. Body waves in poroelastic media saturated by two immiscible fluids, *J. geophys. Res. (Solid Earth),* **101,** 25 149–25 159.

Urquizu, M. & Correig, A.M., 2004. On the equivalence between stratified media and oscillators, *Geophys. J. Int.,* **157,** 245–250.

Virieux, J., 1986. P-SV wave propagation in heterogeneous media: velocity-stress finite-difference method, *Geophysics,* **51,** 889–901.

Walker, D., 2008. Recent developments in low frequency spectral analysis of passive seismic data, *First Break,* **26,** 65–72.

Wei, C. & Muraleetharan, K.K., 2002. A continuum theory of porous media saturated by multiple immiscible fluids, I: linear poroelasticity, *Int. J. Eng. Sci.,* **40,** 1807–1833.

Werby, M.F. & Gaunaurd, G.C., 1989. Broadside resonance scattering from elastic spheroids, *IEEE J. Ocean. Eng.,* **14,** 400–406.

Werby, M.F. & Gaunaurd, G.C., 1990. Resonance scattering from submerged elastic spheroids of high aspect ratios and its three-dimensional interpretation, *J. acoust. Soc. Am.,* **88,** 951–960.

White, J.E., 1975. Computed seismic speeds and attenuation in rocks with partial gas saturation, *Geophysics,* **40,** 224–232.

White, J.E., Mikhaylova, N.G. & Lyakhovitsky, F.M., 1975. Low-frequency seismic waves in fluid-saturated layered rocks, *Izvestija Academy of Science USSR, Phys. Solid Earth,* **11,** 654–659.